Chapter 4

System Hardware and Post-Processing

A measurement system was constructed to observe the cross-correlation of fading and theoretical capacity of spatially separated propagation channels. The system contains sixteen transmitter and sixteen receiver antennas, producing a total of 256 propagation channels. A carrier wave signal is emitted from each transmitter antenna, and a sampled waveform is recorded from each receiver antenna. The waveform from each of the sixteen receiver antennas contains a linear combination of all of the transmitted signals. By emitting a distinct frequency from each transmitter antenna, the measurement system's receiver can use the Fourier transform calculation to separate the transmitted signals from the sampled waveform. Using the assumption of constant transmitter amplitudes, the channel gains can be estimated from this received spectrum and used to calculate MEA capacity and cross-channel correlation, as defined in Chapter 3. The transmitted frequencies are restricted to a 32kHz bandwidth, at 2111MHz, to preserve a narrowband channel model in these calculations.

Two particular system requirements associated with correlation measurements include a low level of mutual coupling between internal components and a high received signal-to-noise ratio. Mutual coupling can result in exaggerated correlation values, while an

inadequate signal-to-noise ratio will reduce correlation and produce equally misleading results. To mitigate these errors, a minimum signal-to-noise ratio requirement of 30dB was maintained. All coupling and distortion products were required to fall below this maximum noise power. Sources of coupling include the power supply and direct radio propagation between unshielded components, as well as the closely spaced elements on the antenna arrays. This chapter describes the system design and significant techniques and algorithms used to simplify implementation and maintain these system requirements.

The design for this measurement system was provided by Peter Wolniansky, currently employed with Lucent Technologies, Bell Labs. With a few discrepancies, this system is a replica of the measurement system completed by Mr. Wolniansky during the Spring 2001 semester. The Lucent measurement system was designed for an outdoor measurement campaign, and several modifications on the original design were necessary to adapt the design for the indoor environment. Due to the concurrent construction of the two systems, discrepancies also exist in the placement of receiver components, in the design of the antenna arrays and in the post-processing software. The measurement system presented in this chapter represents a modified version of the system currently deployed at Lucent Technologies.

4.1 Transmitter Hardware

The transmitter contains sixteen independent signal chains, each producing a single narrowband tone between 2111.002MHz and 2111.032MHz. As shown in Figure (4-1), each parallel chain contains a direct digital synthesizer, generating a preprogrammed baseband tone. This tone is upconverted by a common local oscillator frequency, amplified and transmitted from a single element on the transmitter array. Components shared between signal chains include the local oscillator, the GPS reference oscillator and the power supplies. These components constitute potential sources of mutual coupling in this design.

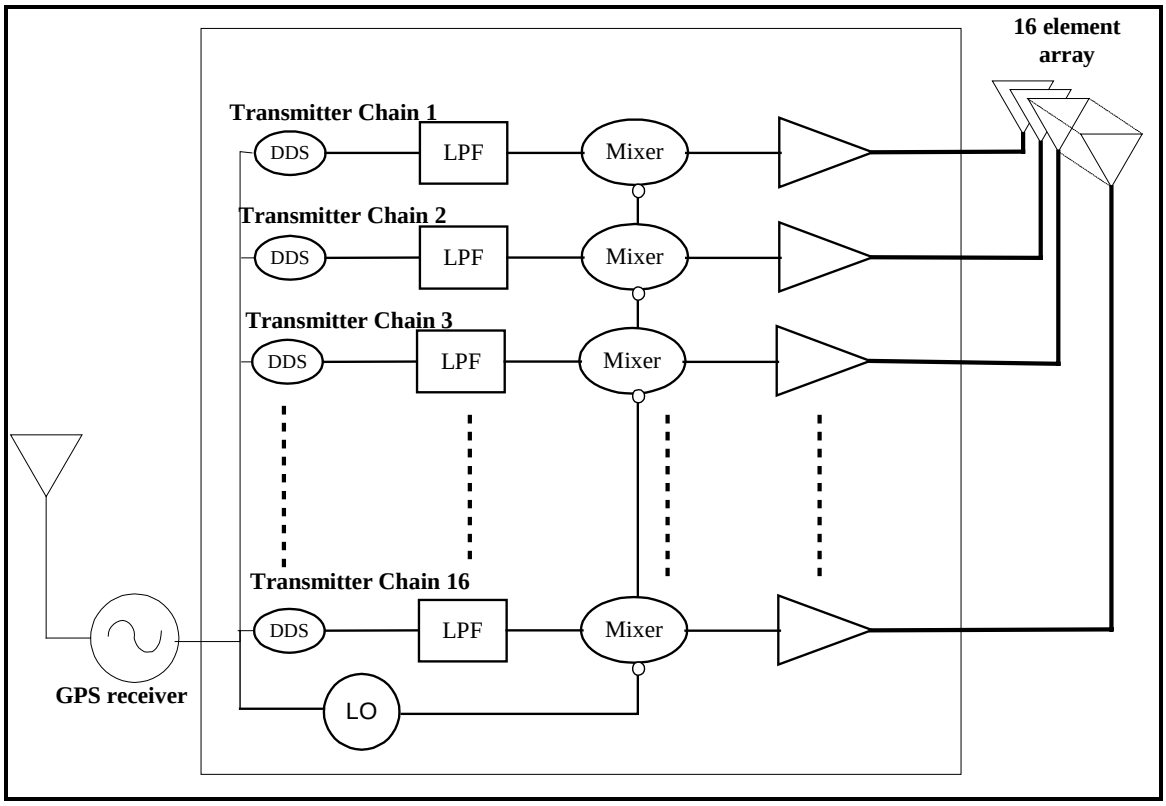

Figure 4-1: Block diagram of sixteen independent transmitter chains. Chains are synchronized by a GPS receiver. RF signals are emitted from a sixteen-element antenna array.

Each of the sixteen transmitter chains produces a sinusoidal waveform of a specific frequency, as specified in Table (4-1). At the output of the direct digital synthesizers (DDS), these frequencies are spaced 2kHz apart, at approximately 1MHz. This spacing is preserved in the upconversion process and defines the total bandwidth of the transmitted signals. It should be noted that, in addition to the low-pass filter shown in Figure 4-1, the DDS output is also conditioned by an RC high-pass filter to block an undesired DC voltage. A DC offset, common in digital-to-analog converters with voltage outputs, can mix with the LO signal to produce an interferer in the transmitter output [40]. The 1MHz frequency offset in the DDS output simplifies the passband requirements of this filter, permitting the use of a single-pole RC circuit with a corner frequency of 500Hz.

The transmitter chains may be thought of as independent users in a multiple-access network. Frequency diversity is employed to identify the transmitted signals at the

receiver, and the phase noise produced by adjacent tones is analogous to interference between transmitters. This phase noise can potentially reduce the signal-to-noise ratio in the received signal. The average signal power at the DDS output was measured as (-18) dBm at each programmed frequency, with a maximum phase noise of –74 dBc at a 2kHz offset. This phase noise is sufficiently low to satisfy the 30dB signal-to-noise ratio requirement.

Table 4-1: DDS frequencies, transmitted RF frequencies, and downconverted frequencies in the receiver. Each transmitter signal chain is assigned one frequency, with an RF frequency spacing of 2kHz and a total system bandwidth of 32kHz. The upconversion and downconversion procedures are depicted in Figure (4-2) and Figure (4-10).

Transmitter number(=i)	DDS output [MHz]	RF frequency [MHz]	Rx baseband [kHz]
1	1.002	2111.002	2.0
2	1.004	2111.004	4.0
3	1.006	2111.006	6.0
4	1.008	2111.008	8.0
5	1.010	2111.010	10.0
6	1.012	2111.012	12.0
7	1.014	2111.014	14.0
8	1.016	2111.016	16.0
9	1.018	2111.018	18.0
10	1.020	2111.020	20.0
11	1.022	2111.022	22.0
12	1.024	2111.024	24.0
13	1.026	2111.026	26.0
14	1.028	2111.028	28.0
15	1.030	2111.030	30.0
16	1.032	2111.032	32.0

Each DDS is referenced to the 10MHz GPS-disciplined oscillator and produces a preprogrammed carrier wave tone, specific to the transmitter number, “i”, as specified in the above table. The transmitter numbers are also included in the frequency expressions in the block diagram of Figure (4-2). This diagram depicts a specific signal chain and includes significant gain and noise figure specifications. The DDS signal is passed through a low pass filter (LPF) and input into the mixer’s IF port. The low pass filter has a 3dB cutoff frequency at 14MHz and over 20dB attenuation at frequencies above

19MHz. This filter attenuates the high frequency signals that may have coupled into the DDS circuit boards through radiation or through the power supply network and prevents distortion in the upconversion and amplification stages. All subsequent components in the signal chain are shielded and contain low-pass filters in series with their power supply inputs to attenuate RF leakage.

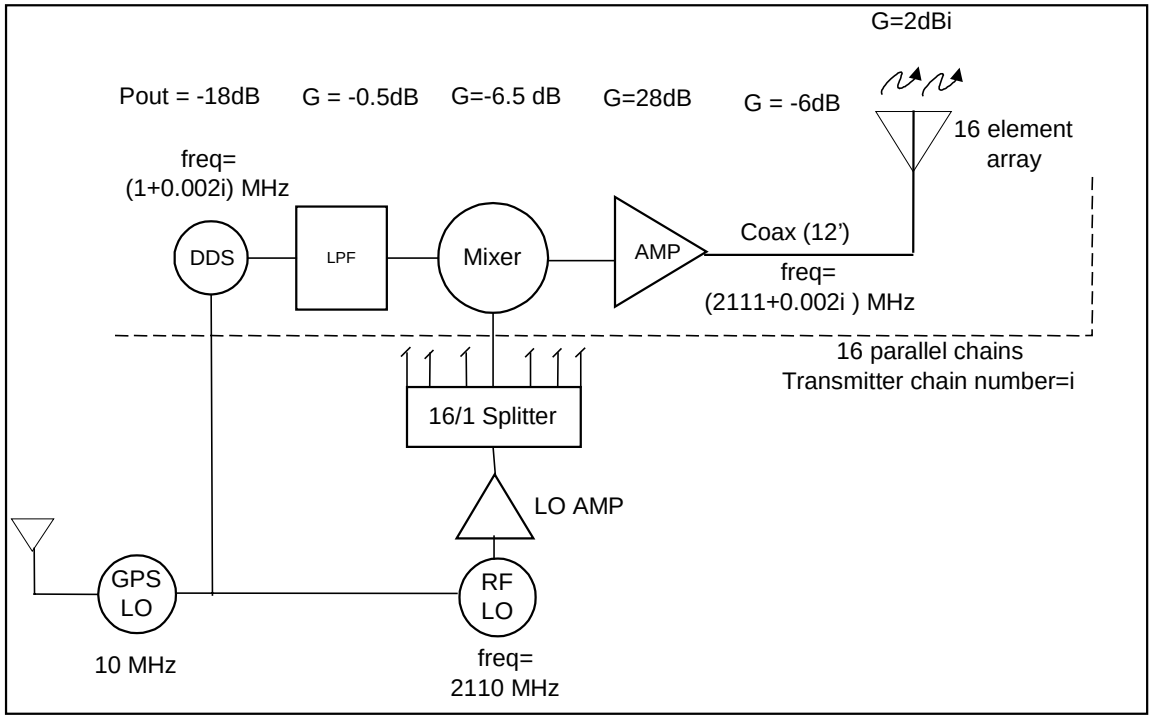

Figure 4-2: Transmitter Block Diagram – The transmitter consists of sixteen independent RF chains. The synthesizers produces tones spaced 2kHz apart. These baseband signals are upconverted, amplified and transmitted from the 16-element array. Specified gains do not include cable loss.

Passive mixers have been shown to exhibit superior linearity in broadband applications when compared to active mixer circuits, but suffer from a higher conversion loss between the IF and RF ports [41]. Linearity may be a concern if this system is converted into a communications testbed or modified for wideband measurements. To accommodate for future upgrades, upconversion of the baseband tones is accomplished with a passive double-balanced mixer. Double-balanced mixers contain differential terminals on all input and output ports to suppress feedthrough of LO and RF input signals [42].

The isolation provided by a double-balanced mixer prevents the LO signal from feeding back into the DDS boards or forward into the RF ports. The LO leakage of the mixer is specified by the manufacturer with minimum and typical values of 38dB and 55dB. The input power on the mixer's LO and IF ports are approximately +10dBm and –19dBm respectively. Attenuation of the LO tone is required to prevent damage to the subsequent amplifier stage. In addition, oscillator feedthrough that is transmitted along with the desired signal acts as a jammer at the receiver. Isolation of the local oscillator port limits the jammer's power and reduces harmonic distortion in the receiver's active components.

After upconversion, each RF signal is amplified and passed through a 12' coaxial cable to its corresponding transmitter array element. The amplifier and cable have gains of 28dB and –6dB respectively, and produce approximately –4dBm at the antenna input. The transmitter emits a double-sideband suppressed-carrier signal, but since the lower sideband is filtered by the receiver. The signal of interest consists of the upper sideband from each transmitter chain, depicted in Figure (4-3).

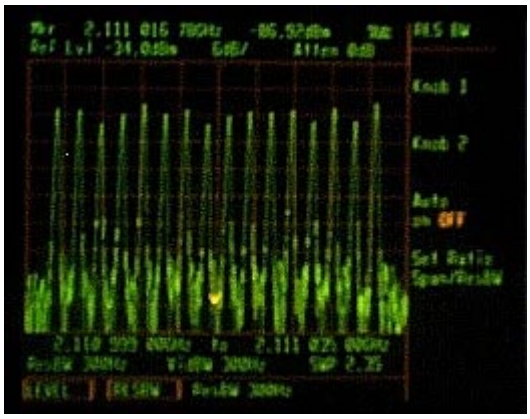

Figure 4-3: Photo of transmitted spectrum, combined from all transmitter antenna elements. The spectrum consists of sixteen narrowband tones within a 32kHz bandwidth.

Considerable effort was expended to maintain a low local-oscillator phase noise and suppress feedback of the RF signals into the LO. As discussed in reference to the digital synthesizers, phase noise produced by the LO broadens the frequency spectrum of each narrowband tone and increases the interference between transmitter chains. Both the transmitter and receiver local-oscillators are encapsulated inside metal enclosures with

the edges sealed with copper tape. The enclosures are also cushioned to reduce mechanical disturbances. These oscillators are tunable from 2000MHz to 2500MHz in 100kHz steps, and are phase locked to a 10MHz reference frequency produced by the GPS disciplined oven-oscillator. The phase noise of the transmitted signal was measured as -50dBc at a 2kHz offset.

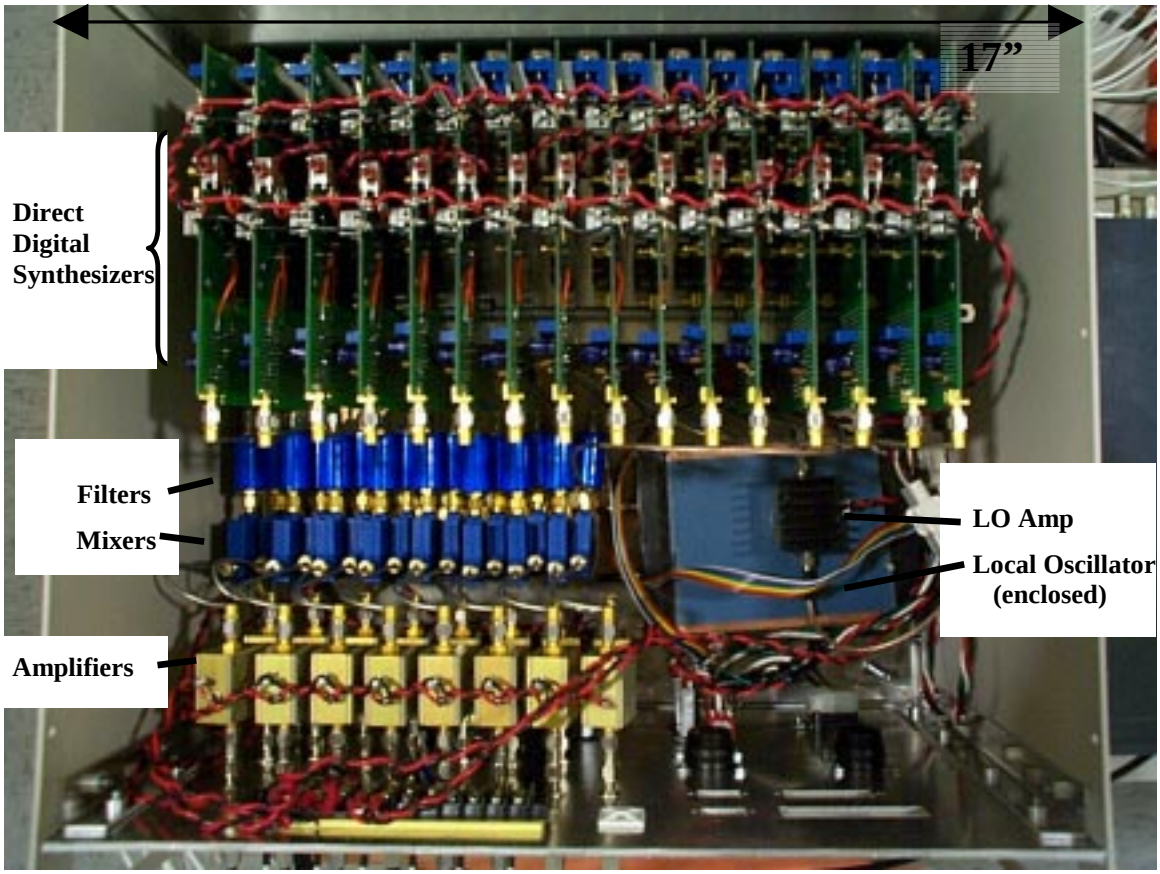

Figure 4-4: Transmitter subsystem. Significant components are labeled.

4.2 Antenna Arrays

The transmitter and receiver arrays each consist of sixteen patch antennas mounted flush on a copper ground plane. On each array, a single signal chain is connected with an antenna element in the arrangement depicted in Figure (4-5). This arrangement is arbitrary, but the labels are necessary in identifying the polarizations and positions of each antenna in the data analysis. The arrows designate the antenna element’s horizontal

or vertical polarization and are drawn on the actual antennas. Each of the sixteen patch antennas on an array consists of a 3-layer printed circuit board, with a rectangular antenna aperture in the top layer. The rectangular aperture is outlined by a groundplane, fed by a rear-mounted adapter and designed with a center frequency of 2.11GHz and a half-power bandwidth of approximately 5MHz. The receiver uses this bandwidth as a front-end bandpass filter to attenuate out-of-band interferers. The elements are arranged with a 0.75λ spacing between the centers of the adjacent patches.

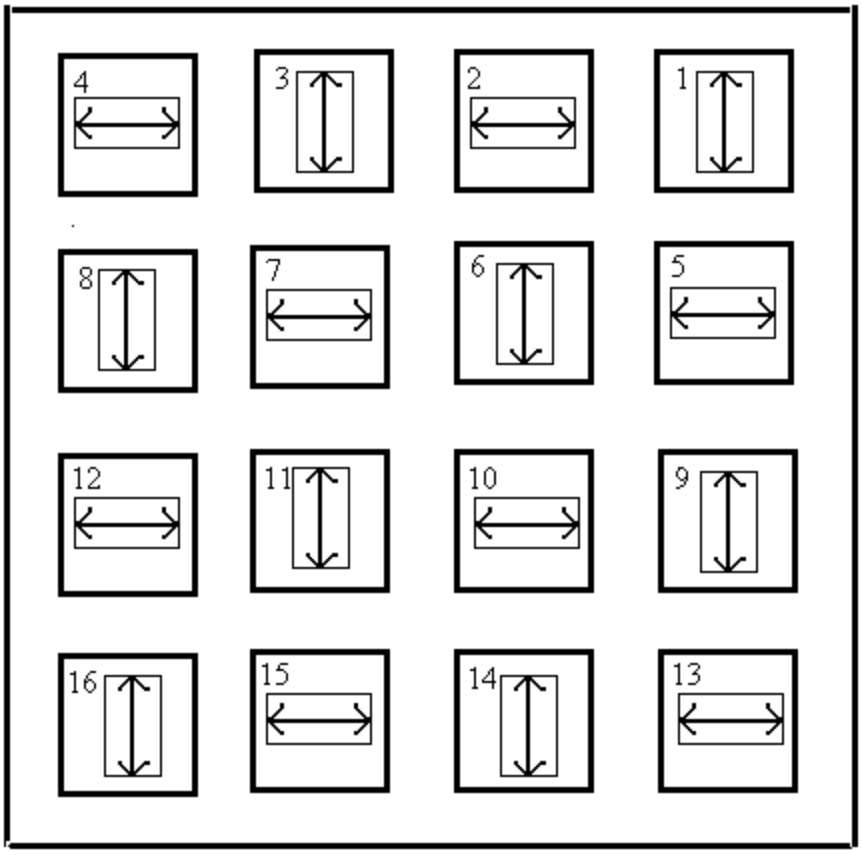

Figure 4-5: Array configuration as seen with the direction of propagation moving into the page. Each numbered patch antenna is set directly on the copper ground plane. The rectangular aperature of each antenna element is shown as well as arrows representing horizontal and vertical polarizations. Transmitter and receiver arrays have identical arrangements, as indicated by the numbers on each antenna element.

Both the antenna patterns of each array element and the coupling between elements will affect the data measured with these arrays. The constructed measurement system can be used to compare the performance of different arrays in a specific environment, or the performance of one pair of arrays in many propagation environments. With this perspective, both the propagation environment and the utilized antenna arrays are independent variables in a measurement campaign. Although coupling between array elements was not analyzed in this investigation, the antenna patterns of many individual elements was characterized.

Measurements were conducted in an anechoic chamber at Lucent's New Jersey location to record the antenna patterns of selected array elements. The array under test was identical to the arrays constructed in this investigation, with the exception of the groundplane material. The tested array had an aluminum groundplane while these were produced with copper groundplanes. The tested array and the arrays built for this measurement system have the same dimensions and identical printed circuit-board elements.

Antenna gain was recorded by feeding a CW signal into a single antenna element with the other elements unterminated. The array was spun around both its azimuth and elevation axes. The two antenna patterns are expected to contain different beamwidths due to the difference in vertical and horizontal lengths of the antenna aperture. Figure (4-6) depicts the antenna pattern of the number 16 element, and presents a good example of the observed characteristics for all of the antenna patterns. The main beam was observed to have an average broadside gain of 2dBi with a ripple of no more than +/- 2dBi from this mean value.

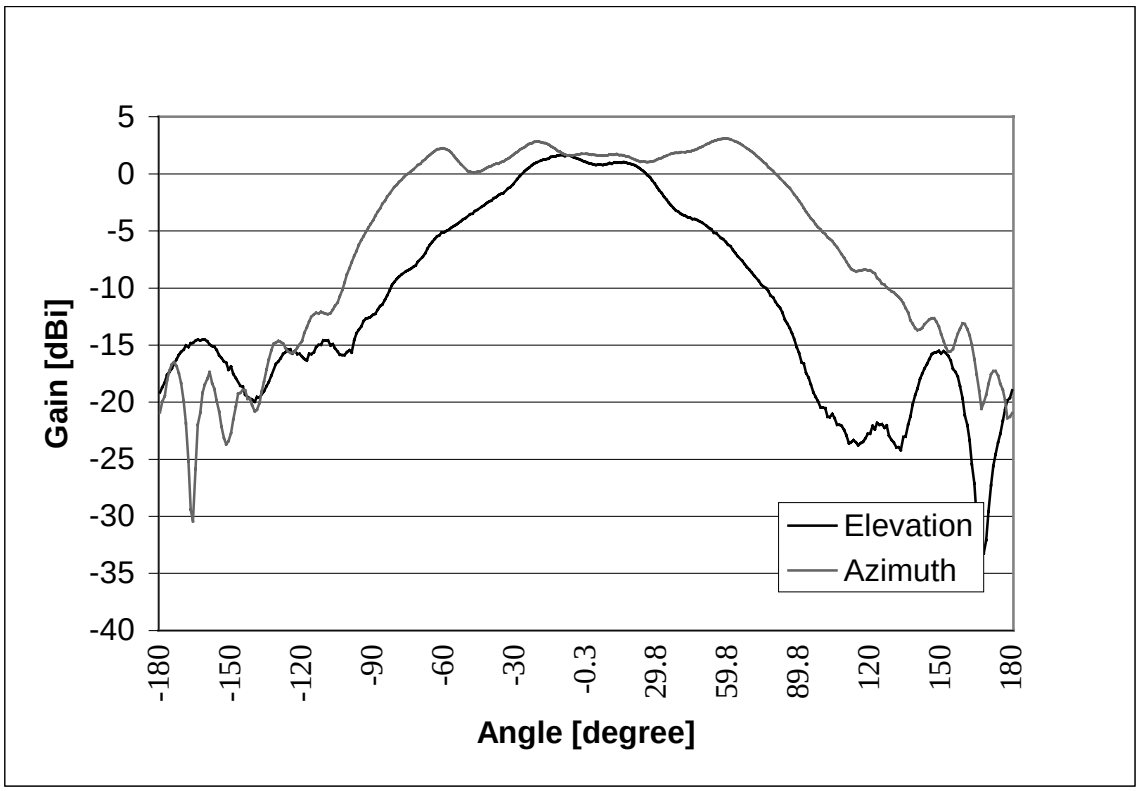

Figure 4-6: Antenna pattern of element 16. The half-power beamwidth is approximately +/- 80 degrees in the azimuth and +/-30 degrees in the elevation. A ripple of about 3 dBi was observed in the main beam of the majority of measured antennas.

It can be observed in Figure 4-6 that the number 16 element has a half-power beamwidth of approximately +/- 80 degrees in the azimuth and +/-30 degrees in the elevation directions. Similar beamwidths were observed in the majority of the vertically polarized antennas. Because the elevation and azimuth axes were defined for the entire array in this measurement, these beamwidth specifications are reversed for the horizontally polarized elements. Each antenna produced a wide beamwidth when spun around the axis defined by its narrow dimension, and visa versa.

Ideal antennas with rectangular apertures have been demonstrated to produce beamwidths proportional to the dimensions of their aperture. Equation (4-1) describes the half-power beamwidth (HP) in terms of the propagation wavelength and antenna dimensions, and can be used to substantiate characteristics observed in the measured antenna patterns.

The dimension “L” denotes the length of the aperture parallel to the direction of the beamwidth measurement. On the measured array, a vertically polarized element has a height of 2.25inches and a width of 1.125inches. These dimensions produce calculated beamwidths of +/-60 and +/-115 degrees in the elevation and azimuth directions respectively. The discrepancy between the theoretical and measured beamwidths may be due to an imperfect antenna groundplane or the practical limitations of printed circuit board construction [43].

$$HP = 0.886\frac{\lambda}{L} \text{ [radians]} \qquad \textbf{(4-1)}$$

In addition to a non-ideal beamwidth, the antenna pattern also contains a ripple in the main beam, with periodic maximum and minimum points. This periodic function indicates that, although most of the transmitted energy radiates directly from the patch antenna, a significant amount of energy may radiate from the non-ideal array groundplane. Using Equation (4-1), the observed period in the antenna ripple of 15 degrees corresponds to a length of approximately 1.4 feet. This result matches the actual dimensions of the array backplane of 1.3 feet by 1.3 feet, and it suggests that the transmitted signal from each antenna element was coupled into the backplane and radiated from the backplane surface. The superposition of this secondary transmission on the main beam may have produced the observed antenna pattern ripple. Sources of mutual coupling, between antenna elements and between elements and the common groundplane, can degrade the integrity of correlation measurements. If the transmitted frequency from one signal chain couples between antenna elements, the observed cross-correlation between the respective pair of propagation channels would be exaggerated in the recorded data. Non-ideal characteristics of the antenna arrays may constitute a source of error in this measurement system.

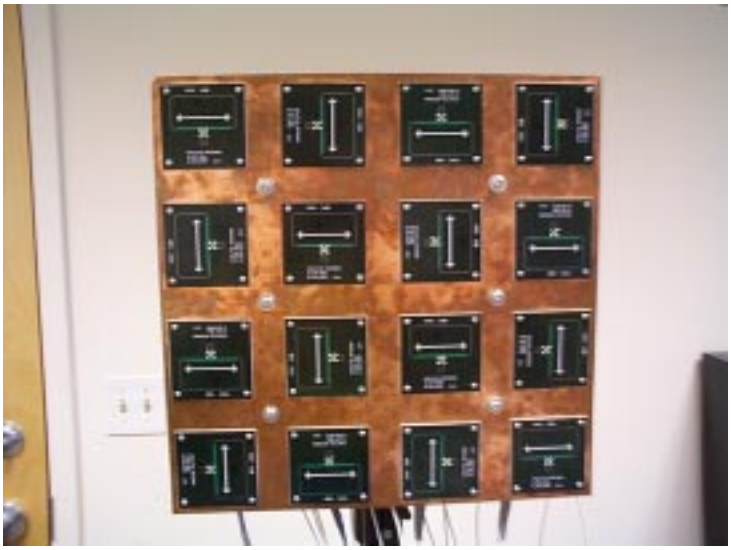

Figure 4-7: Photograph of the receiver antenna array, with dimensions of 1.3' by 1.3'. The arrows on each element indicate polarization.

4.3 Receiver Hardware

The receiver consists of sixteen parallel signal chains as shown in Figure (4-8). Each chain is connected to a single antenna on the receiver array through a 12' coaxial cable. The sixteen inputs are independently amplified, downconverted and filtered to produce thirty-two quadrature baseband signals. The quadrature chains are denoted as I and Q for each receiver antenna in Figure 4-8. These signals are then sampled by analog-to-digital converters, multiplexed and saved to a binary file. Each sampled signal contains the sixteen transmitted tones, with equally spaced frequencies from 2kHz to 32kHz.

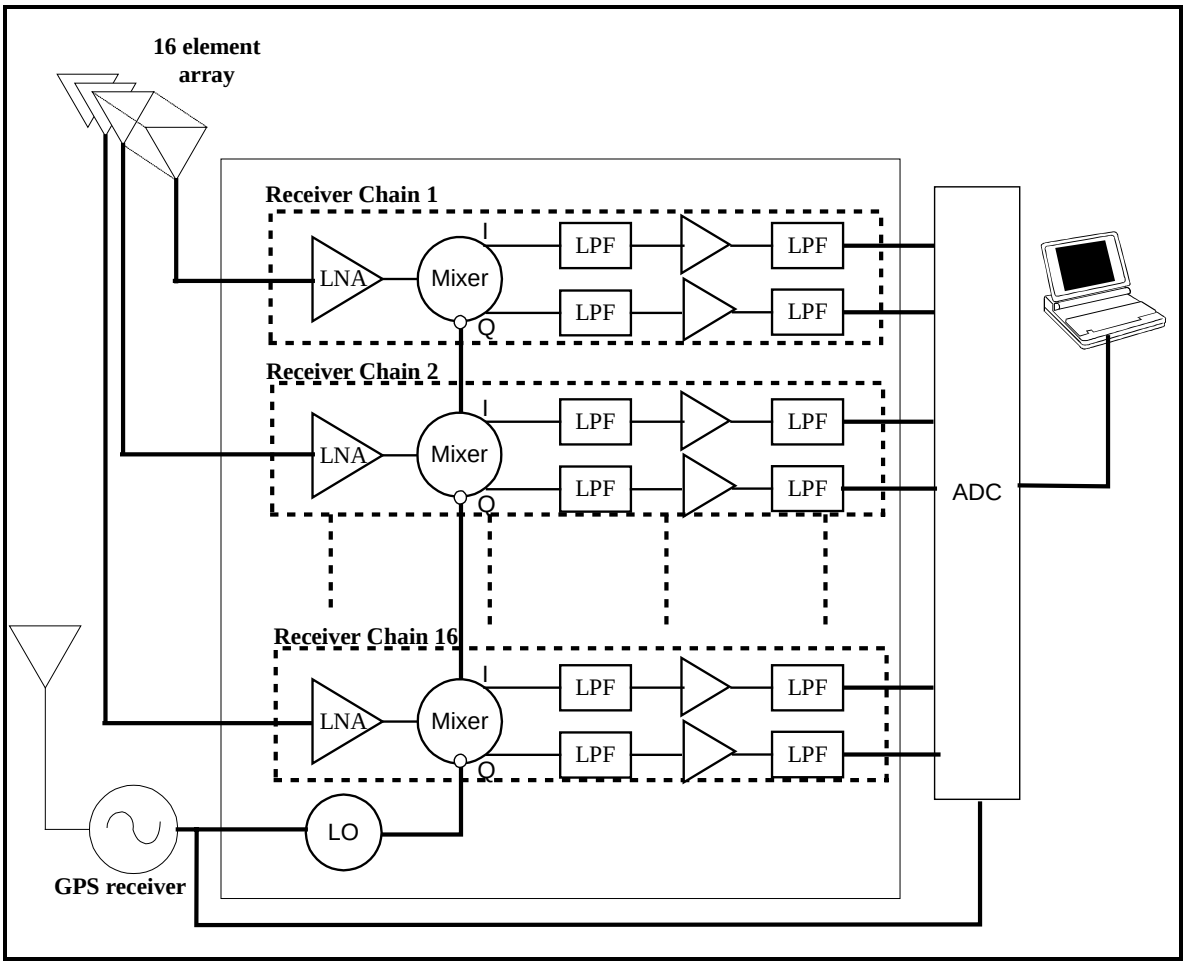

Figure 4-8: Block diagram of 16 independent receiver chains.

Both the GPS reference and the local oscillator are identical to their counterparts in the transmitter subsystem. The 10MHz GPS signal acts as a reference for both the oscillator and the analog-to-digital converters, and minimizes frequency drift between the transmitter and receiver. As in the transmitter, the local oscillator is packaged and cushioned to limit spurious components and excessive phase noise in the output signal. The oscillator output is amplified, split into sixteen equal power components and passed to the downconversion mixers. A sample receiver chain is depicted in the following diagram, including significant gain and noise figure specifications.

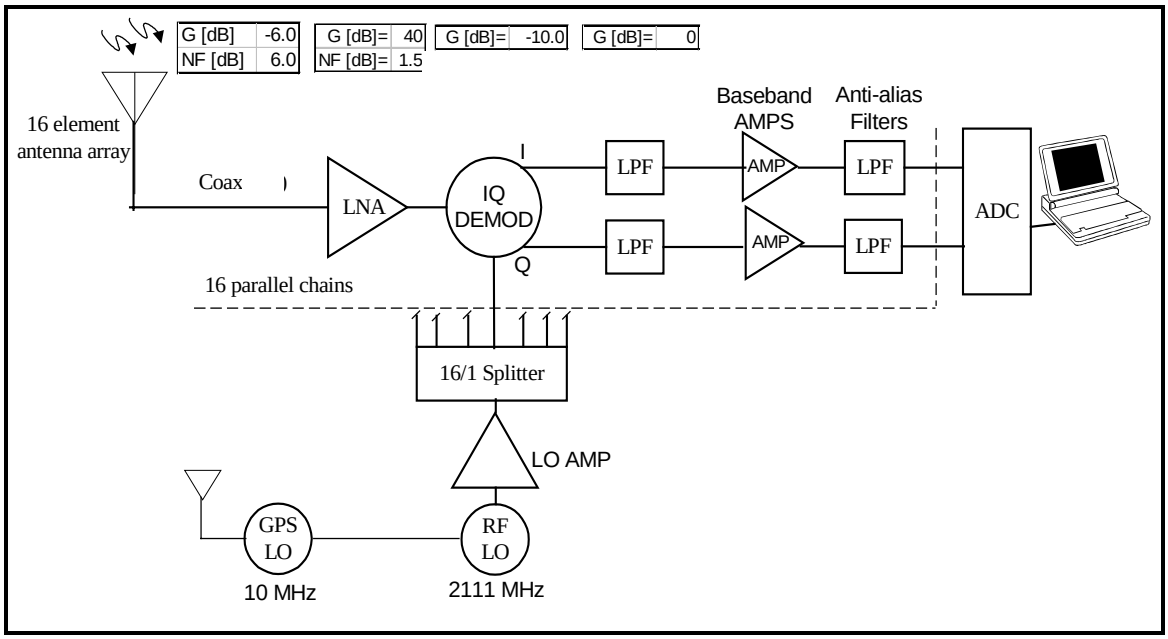

Figure 4-9: Block diagram of one receiver chain. Cable losses are not specified in this figure.

The foremost concern in the design of a measurement system focuses on the quantity of noise in the recorded data. Equation (4-2) relates the total noise figure of a cascaded network to the gain and noise figure specifications of its individual components. This equation suggests that the contribution of a component's noise figure to the total noise figure is determined by the cumulative gain of previous components. Placing low-noise amplifiers at the beginning of a receiver's signal chain minimizes noise figure and preserves the signal-to-noise ratio of the sampled signal. In Figure (4-9), a pair of cascaded low-noise amplifiers have been combined into one component block and specified with a total gain of 40dB and a noise figure of 1.5dB. This amplification produces a positive cumulative gain in all subsequent stages and makes the noise figure contribution of the latter components insignificant [8].

$$NF_{TOT} = 1 + (NF_1 - 1) + \frac{NF_2 - 1}{G_1} + \frac{NF_3 - 1}{G_1 G_2} + \ldots \qquad \textbf{(4-2)}$$

Equation 4-2 suggests that the bulk of the total noise figure is contributed by the first component in the signal chain, the coaxial cable connecting the antenna outputs to the low-noise amplifier. This cable is characterized with a 6dB noise figure, but is necessary

to provide the freedom of movement required for measurement campaigns. A reduced noise figure could have been produced by placing the low-noise amplifiers directly following the antennas, but this would have required lengthy power cables, further complicating the design. In addition, it was decided that the amplifiers must be shielded by the receiver enclosure to prevent leakage from the transmitter or other interfering systems. A 6dB degradation in signal-to-noise ratio is considered an acceptable cost for long cable lengths, and the required 30dB signal-to-noise ratio in the recorded data has been achieved with this configuration. A detailed noise figure analysis is presented in Chapter 5.

After amplification, the signal is downconverted and split into its in-phase and quadrature components with quadrature type mixers. These passive mixers are specified with a conversion gain of –10dB. The system is designed to produce complex H-matrix elements from the sampled quadrature signals by combining the amplitudes of these components in the data processing. Subsequent audio stages including the digital-to-analog converter in the data acquisition subsystem, contain 32 in-phase and quadrature signal chains.

It should be noted from the transmitter and receiver block diagrams that the two local oscillators are offset by 1MHz. This offset is used to separate the sidebands of the transmitted signal, as depicted in Figure (4-10). In the transmitter, each DDS produces a narrowband signal with a frequency close to 1MHz. The combination of these signals can be referred to as the baseband source. In upconversion, upper and lower sidebands are produced around the 2110MHz transmitter local-oscillator frequency, as depicted at the top of Figure (4-10). Each sideband is spaced approximately 1MHz from the LO and contains a 32kHz bandwidth, after combining all transmitted signals. By placing the receiver LO frequency at the edge of the upper sideband, this sideband will be adjacent to the 0MHz frequency axis in the downconverted signal, as illustrated at the bottom of the figure. A low-pass filter can then be used to attenuate the lower sideband and isolate the desired 32kHz bandwidth. In this system, a double-sideband signal is generated to avoid

complexity in the transmitter design, and one sideband is filtered in the receiver to maintain a narrow 32kHz system bandwidth.

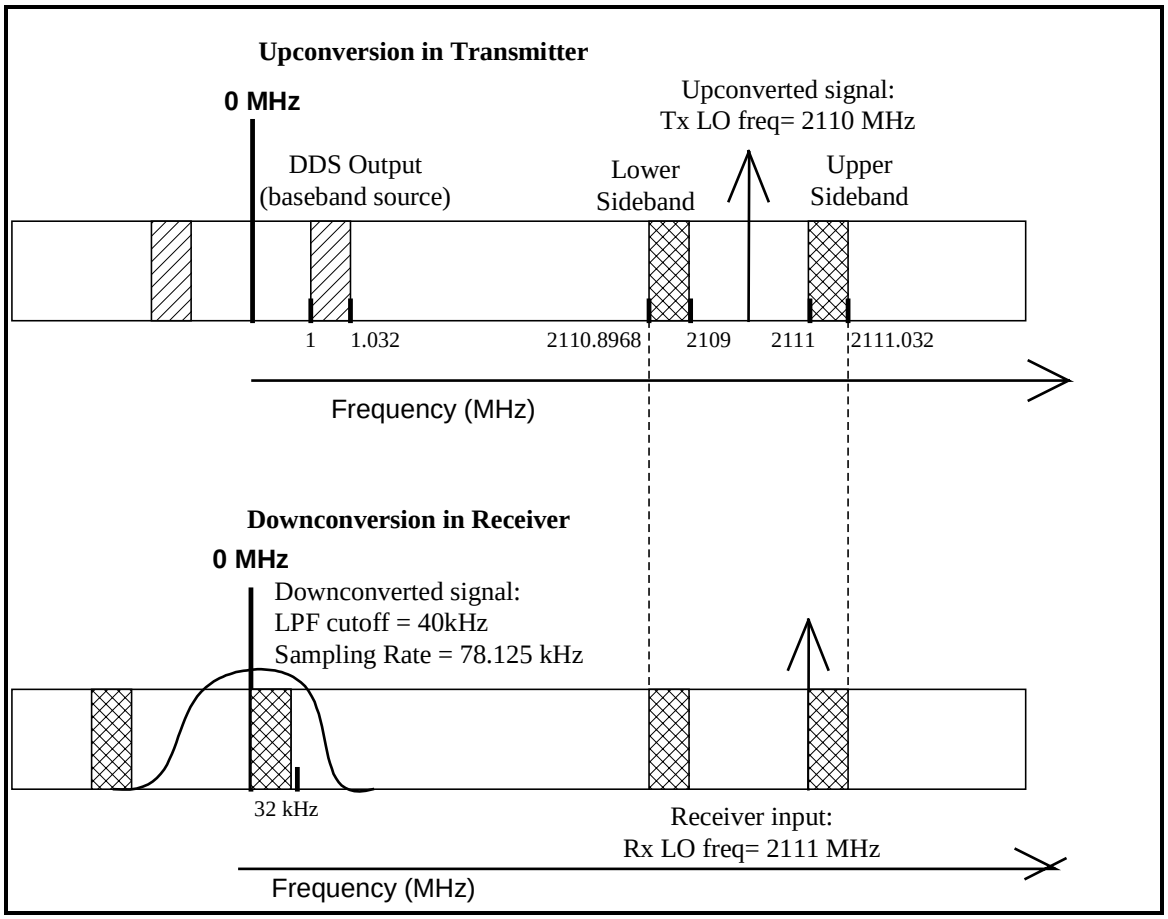

Figure 4-10: System frequency diagram: The baseband source is upconverted in the transmitter and the double-sideband signal is downconverted in the receiver. Different local oscillator frequencies in the transmitter and receiver are used to isolate the upper sideband after downconversion with a low pass filter.

The receiver contains two low-pass filter stages, one preceding and one following the audio amplifiers. The first filter is specified with a 14MHz half-power bandwidth and isolates subsequent stages from high frequency feedthrough originating from the mixer's RF or LO inputs. The filter also attenuates signals reflected by the high load impedances in the audio components. This filter is specified with less than 0.5dB loss at frequencies up to 11MHz and greater than 40dB loss at frequencies higher than 24MHz.

The audio amplifiers are used to drive the high impedance inputs of the second filter stage. The amplifiers contain a 50Ohm input impedance, a 10kOhm output impedance and drive an impedance of 1MOhm at the input to the anti-aliasing filters. A voltage gain of 12 was measured between the input and output loads, which translates into a power gain of –1.4dB across a 10kOhm impedance, using Equation (4-3) [6].

$$P_{IN}[dB] - P_{OUT}[dB] = 10\log_{10}\left(\frac{(V_{OUT})^2 \frac{1000mW}{1W \cdot 10k\Omega}}{(V_{IN})^2 \frac{1000mW}{1W \cdot 50\Omega}}\right) \quad \textbf{(4-3)}$$

The audio amplifier's gain may be misleading when specified in terms of power because audio components often contain high input and low output impedances to efficiently transfer signal voltages between cascaded stages [6]. Even though the audio amplifier produces a power loss, the voltage gain of 12V/V increases the signal voltage measured by the analog-to-digital converter and recorded in the sampled data. As a note, the anti-aliasing filter contains a 1MOhm input and an internal buffer stage specified with a 1Ohm output impedance. The analog-to-digital converter contains a 10kOhm input impedance.

The second low-pass filtering stage prevents aliasing in the sampled data by limiting the signal bandwidth. The Nyquist Theorem states that aliasing, or undersampling, occurs if the signal bandwidth is greater than half the sampling frequency of the analog-to-digital converters (ADC). In the receiver, anti-aliasing filters immediately precede the ADC to bandlimit the sampled waveform and satisfy the Nyquist requirement. The filters are designed for gain flatness in the passband, to minimize distortion of the desired waveform, and large stopband attenuation. The anti-aliasing filters used in this measurement system are characterized by a low-pass 8-pole Butterworth reseponse with a 3dB bandwidth of 40kHz. The bandwidth was chosen to minimize distortion of the transmitted signal, even though it is wider than the required Nyquist bandwidth. The Nyquist requirement is satisfied because the transmitted signal consists of only narrowband tones within the Nyquist bandwidth and no interfering signals are present with a significant power level.

The anti-aliasing filters were chosen to minimize distortion of the transmitted signal. The Butterworth filter response produces a flat magnitude response in the passband, but at the cost of a large group delay due to a nonlinear phase response. A group delay can be observed as ringing or intersymbol interference in the filtered signal [40]. This system compensates for the nonlinear phase response by normalizing the received spectrum in the post-processing. The Butterworth filters have a half-power bandwidth of 40kHz, with 18dB of attenuation at 52kHz and 48dB attenuation at 80kHz. The high-order filters minimize the attenuation of the desired 32kHz bandwidth signal while removing undesired signals outside the Nyquist bandwidth.

Direct-downconversion receivers are commonly susceptible to slowly changing DC offsets in the mixer output, due to leakage of the oscillator signal into the low noise amplifier. The downconverted signal of the LO mixed with itself has a 0Hz frequency, and may produce clipping in the audio components or the analog-to-digital converter. In many communication systems, this signal cannot be filtered out without also attenuating low frequency components of the data [8]. Because this measurement system does not utilize the bandwidth below 2kHz, high-pass filters can be implemented at the audio amplifier and ADC inputs without affecting the amplitude of the low frequency tones. These simple RC filters, omitted from the block diagram, have a knee frequency of 100Hz and prevent low frequency parasitics from saturating these components.

The components depicted in Figure (4-11), and described above, isolate, amplify and downconvert the desired signal from the antenna array inputs. At the output of the anti-aliasing filters, the signal in each chain is composed of narrowband tones between 2kHz and 32kHz with varying amplitudes. The baseband signals are passed to the analog-to-digital converters and the sampled data is stored in a binary file. The data-sampling process is discussed in the next section.

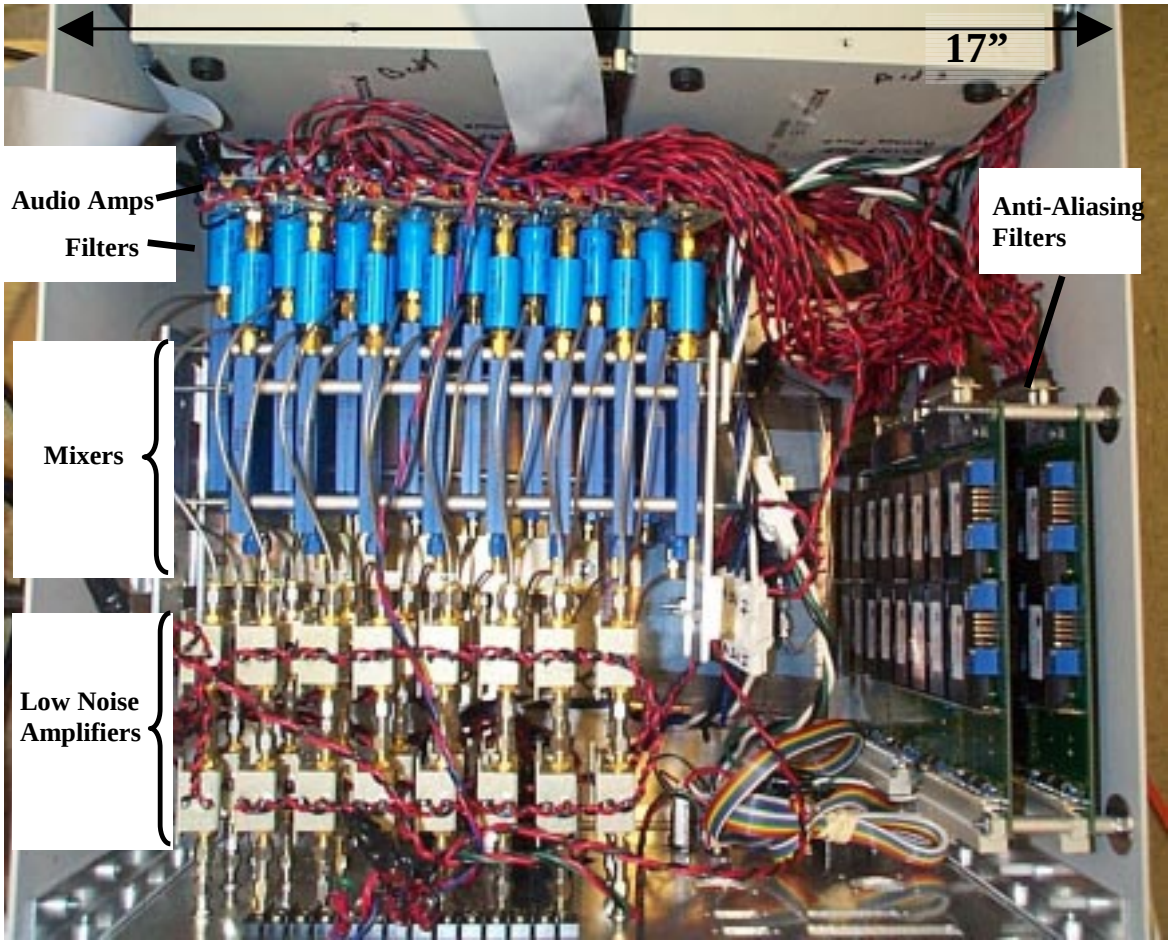

Figure 4-11: Receiver subsystem. Significant components are indicated.

4.4 Data Acquisition

The data acquisition subsystem consists of two National Instruments analog-to-digital converters, controlled using LabVIEW software. LabVIEW is a graphical programming language where data flow is represented by wires and processing blocks are analogous to functional or mathematical circuits. Used primarily for data acquisition applications, this software automates the configuration and operation of the National Instruments components used in this measurement system. These components are installed in a portable computer with dual 600MHz processors and a 73Gigabyte hard-drive. A computer with this processor and hard-drive, 256Mbytes of memory and a SCSI interface was utilized to maximize storage capacity and sampling rate [44].

Each of two analog-to-digital converters, contains sixteen input channels and samples data from one of the 32 quadrature signal chains during each trigger signal period. The receiver's in-phase signal chains are sampled by the first ADC and the quadrature signal chains are sampled by the second. The 10MHz GPS signal is divided by a factor of eight with an internal counter, and the resulting 1.25MHz frequency acts as the trigger input for each ADC. The converters use a round-robin style of acquisition, continuously cycling between the sixteen input channels and collecting 78125 samples from each signal chain per second. The Nyquist sampling theorum states that the sampling rate of an ADC must be at least twice the bandwidth of the input signal to accurately reconstruct the signal in the digital domain [45]. With a 32kHz signal bandwidth, this sampling rate is about 18kHz higher than the minimal Nyquist sampling rate.

Once quantized, the 12-bit sampled data is placed in a circular memory buffer. This type of memory enables the computer to write to one side of the buffer and read to a file from the other side. Although both processes are not simultaneous, they may be performed alternately by different programs operating at the same time. In this way, the computer can take advantage of dual processors to stream data continuously to a binary file from the analog-to-digital converters [46]. With its current storage capacity, the measurement computer can collect three hours of continuous data.

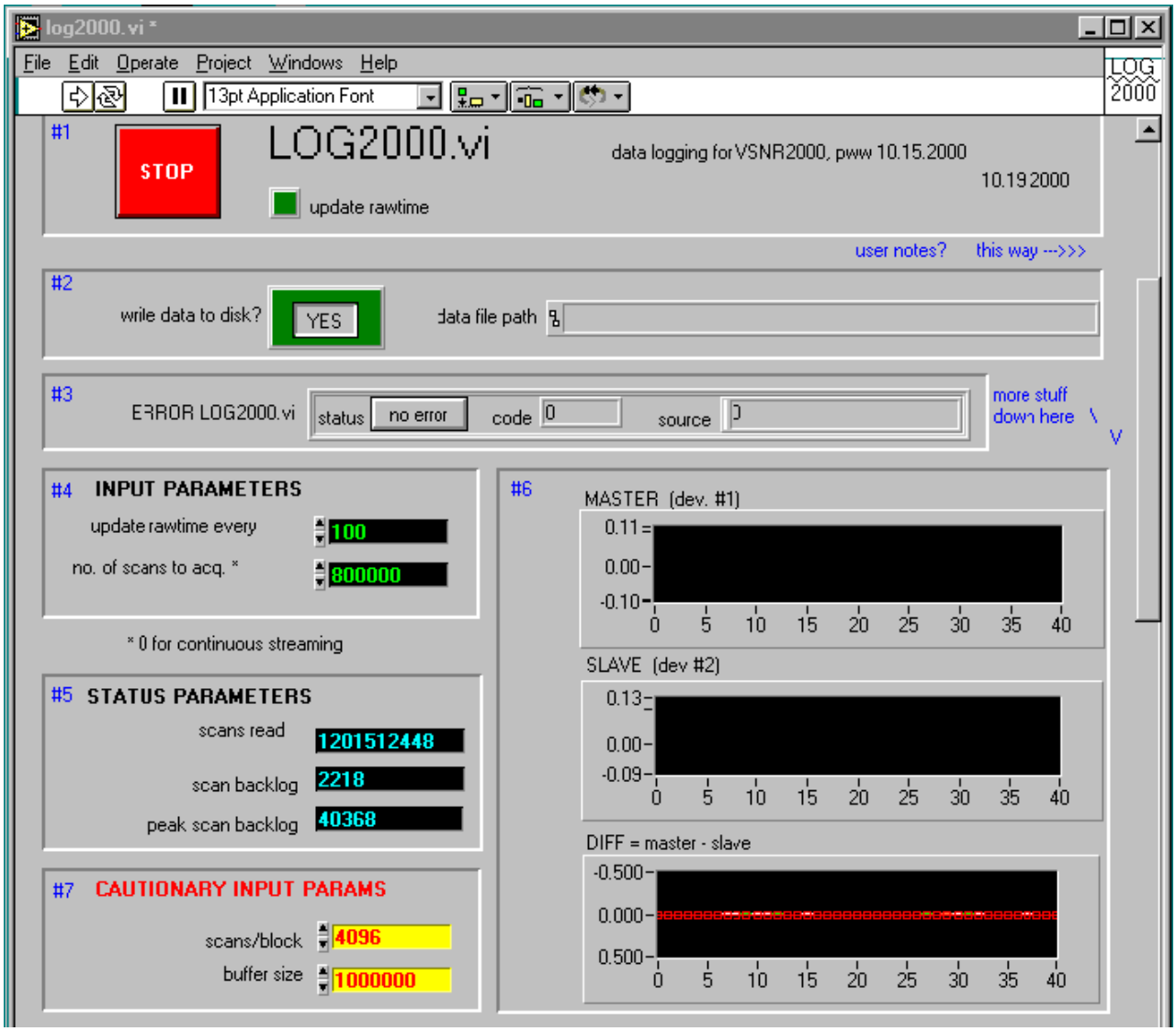

Figure 4-12: Data acquisition software frontpanel. User inputs include number of scans to record, record speed and target file.

4.5 Post-processing

Propagation measurements are often conducted to verify predicted diversity or capacity gains in a particular environment. Two possible methods of obtaining this data are to build a prototype of a specific communication system or to build a measurement system which can be used to characterize the channel in terms of related variables. Because prototype measurements are expensive and often design-specific, investigators usually

defer this option until the final phase of product development. The measurements described in this thesis are applicable to a variety of systems and characterize the indoor environment in terms of cross-channel correlation and theoretical capacity. The following post-processing computations transform the sampled data into H-matrices, with which these parameters can be calculated.

The data-acquisition and post-processing algorithms were implemented with two different fundamental objectives. The acquisition process performs no signal processing or data compression; the sampled voltage levels are stored directly to disk from the input memory buffer. The omission of non-essential processes allows the LabVIEW acquisition software and analog-to-digital converters to sample and save data at the required sampling rate. The remainder of the data processing is performed with the MATLAB programming software after the data acquisition is finished. In this step, processing time is not a priority, and no attempt was made to optimize the program's speed. The post-processing algorithms have been designed to maximize the accuracy of the computed results.

The raw data saved by the data acquisition software contains the concatenated streams of sampled data for all of the signal chains in a 12-bit binary format. First, the binary data is translated into voltage values and reshaped from a stream of concatenated voltage levels into a two-dimensional matrix. This matrix has 32 columns, corresponding to each of the in-phase and quadrature chains, and a predetermined number of rows depending on the duration of the measurement.

Each column of sampled data is then truncated into blocks, where each block represents a short period of time, or time instant. The column in a block is processed with the *Discrete Fourier Transform* (DFT) to obtain the frequency spectrum of the signal received from that column's respective antenna. The Discrete Fourier Transform operates on a signal, represented by a finite number of samples, and produces a discrete spectrum consisting of an equal number of frequency bins. This process is repeated for each signal chain and for each time-block [36].

The number of samples input into the Fourier Transform is designed to place the transmitted frequencies in the middle of the calculated frequency bins. If transmitted spectral components are located between the frequency bins, the power in these spectral components is smeared across a large number of the bins in the output spectrum. This distribution of a narrowband spectral component over a wide range of frequencies is called *spectral leakage* and can result in exaggerated noise power levels [46]. In the Fourier transform output, the frequency bins are evenly distributed between the 0Hz and half of the sampling frequency, Fs, as represented by the sequence [36]:

$$Frequencies = \frac{Fs}{2N}[0:N] \qquad \textbf{(4-1)}$$

The parameter "N" denotes the number of time samples input into the DFT, and must be designed to place all of the transmitted tones at the center of the frequency bins. The minimum value of "N", producing a resolution bandwidth of 2000Hz, places each transmitted tone in an adjacent frequency bin. Acceptable values of "N" can be multiples of this minimum, shrinking the bandwidth of each frequency bin and increasing the number of bins between transmitted tones. These acceptable values, listed in Table 4-2, produce bins aligned with the transmitted frequencies. The resolution bandwidth is the width of a single frequency bin and has been calculated from Equation (4-4) by solving for the spectral distance between the first and second elements.

Table 4-2: Potential size of the Fourier transform input and the corresponding values of resolution bandwidth.

Resolution bandwidth [Hz]	Number of samples (N)
2000	39.0625
1000	78.125
500	156.25
250	312.5
125	625
100	781.25
62.5	1250

The number of acceptable "N" values can be reduced by restricting the time-length of the transform input to the *coherence time* of the channel. The coherence time is the duration over which the channel gain can be assumed constant, and is calculated using the autocorrelation function. Movement of the transmitter, the receiver or scattering objects produce a time-varying amplitude in the received signal, as discussed in Chapter 2. These fluctuations produce a small, random frequency shift in the received signal, often referred to as Doppler shifting. The coherence time describes the duration over which movement in the channel is very small, producing negligible Doppler shift and a high correlation between the amplitudes of two signals passing through a propagation channel at different times. Assuming that the envelope of the received signal has a Rayleigh distribution, the coherence time can be defined as the duration over which the signal has a correlation coefficient greater than 0.5. Calculations of the maximum Doppler shift and coherence time are expressed in terms of maximum velocity of the transmitter, receiver or scatterers, "v" [11]:

$$f_m = v/\lambda \qquad \textbf{(4-5)}$$

$$T_C = 9/16\pi f_m \qquad \textbf{(4-6)}$$

Equation (4-5) relates the maximum velocity of a scatterer in the channel to the maximum Doppler shift. It assumes that the scatterer is moving directly toward or away from the receiver, producing the largest possible frequency shift in the received signal. A maximum predicted velocity of 5mph, produces a maximum Doppler frequency of 16Hz and a coherence time of 0.011sec. This duration corresponds to 889 samples, given a sampling rate of 78125samples/sec. Referring again to Table (4-2), this coherence time prevents the use of a Fourier transform block size with more than 889 samples. To maximize spectral resolution and the signal-to-noise ratio of the calculated spectrum, the largest acceptable block size should be used to calculate the Fourier Transform. By restricting the duration of an input block to the channel coherence time and minimizing the resolution bandwidth, a block length of 781 samples was found to optimize the Fourier transform output spectrum.

Rounding the value of N from 781.25, as specified in Table (4-2), to 781 produces a small frequency offset between the transmitted tones and the center of the output bins, and may reduce the signal-to-noise ratio. It was observed from data recorded in calibration measurements that this block size produces a significantly higher signal-to-noise ratio than the next highest integer of N=625. The calibration measurements are described in Chapter 5.

A windowing function is used to further reduce the level of distortion resulting from the Fourier transform. The discrete Fourier transform uses the assumption than the input signal contains an infinite block length. A finite block length produces ripples in the output spectrum, near the edges of the frequency band. This effect is called the Gibbs phenomenon, and can result in errors in the calculated results. Windowing the waveform input into the DFT function tapers the ends of the sampled data block, removing the abrupt edge that produces these ripples. The Blackman window has the following time-domain transfer function, also depicted in Figure (4-13) [48] [49]:

$$h(n) = 0.42 - 0.5\cos(\frac{2\pi \cdot n}{N-1}) + 0.08\cos(\frac{4\pi \cdot n}{N-1}) \qquad \textbf{(4-7)}$$

In the windowing function, the variable "n" is the time-step index and varies between 0 and (N-1). The Blackman window is characterized by its wide main lobe and low sidelobes, producing low spectral resolution and low levels of spectral leakage. In the resulting Fourier transform, this transfer response will broaden the main spectral component of each transmitted tone but minimize the spread of signal power between the transmitter frequencies. A broad spectral response is usually detrimental to measurement systems because it widens the received spectrum, but this system uses this spectral broadening as an advantage. By spreading the power of each transmitted tone slightly inside a Fourier transform bin, the window minimizes the affects of small offsets between the transmitted frequencies and the centers of the bins [48] [49].

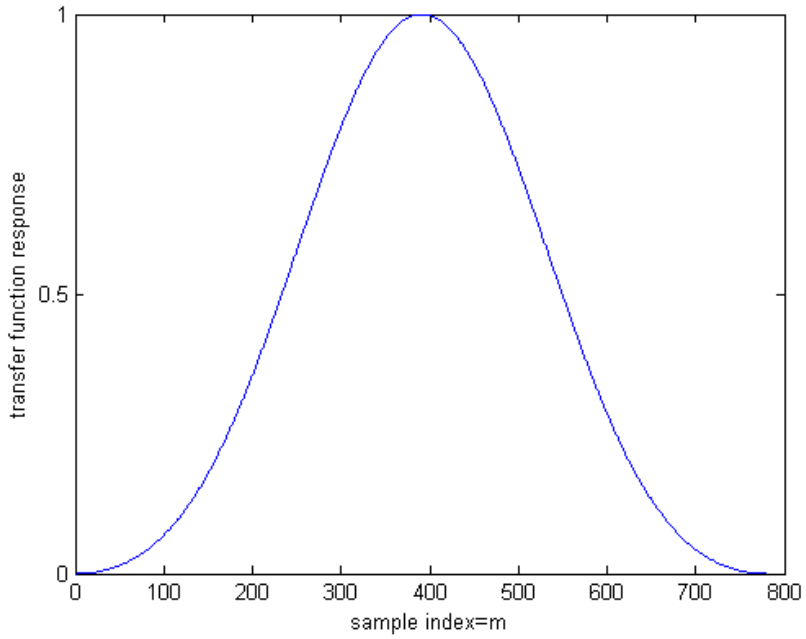

Figure 4-13: Time-domain response of the Blackman Windowing function with N=781.

Figure (4-14) depicts the power spectrum of a single receiver signal chain. Note that each narrowband peak represents the signal from one transmitter. A spectrum is produced for each of the receiver's 32 quadrature signal chains. The amplitudes of each transmitter frequency are picked from each receiver spectrum and combined into the H-matrix, introduced in Chapter 3. After combining the in-phase and quadrature signal chains, the H-matrix has the dimensions of sixteen by sixteen elements, and represents the complex amplitude of the signal at each receiver antenna from each transmitter antenna, at one time instant.

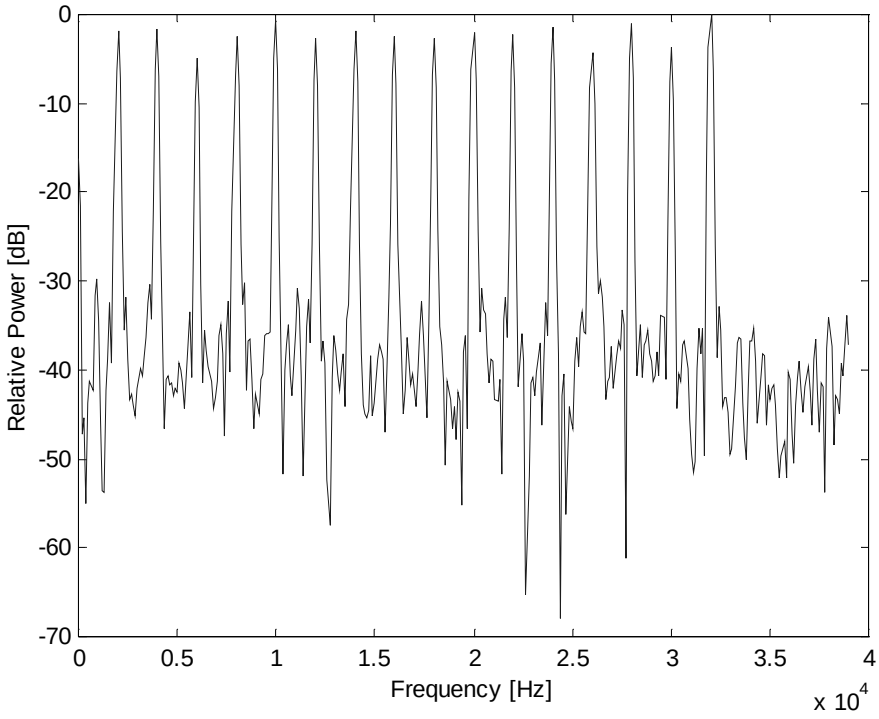

Figure 4-14: Spectrum of a single receiver chain calculated using the FFT. Each peak consists of an individual transmitter component (shown in different colors). This spectrum was recorded during a propagation measurement.

The measurement system used to collect this data has many physical imperfections, and both the gain and phase of the complex amplitudes must be normalized to correct for these factors. As mentioned in the previous section, data is multiplexed in the acquisition process in round-robin format. This produces a temporal offset between the sampling times of each receiver signal chain, which translates into a phase offset in the H-matrix elements. This phase offset can be calculated from the sampling delay and the transmitter signal frequency and appended to the corresponding H-matrix element. The Fourier transform pair expressed in Equation (4-8) relates the effect of a time-shift operation on the frequency spectrum, where X(w) is the Fourier transform of the sequence x(t) [45]:

$$x(t - t_O) = e^{-(jwt_O)} * X(w) \qquad \textbf{(4-8)}$$

The H-matrix must also be normalized to account for unpredictable gain deviations caused by device aging and long-term instability. A daily calibration was designed to characterize the gains of each transmitter and receiver chain in a controlled measurement. From this measurement, a gains-matrix is produced with the same algorithm as described above in producing the H-matrix. Each element in the measured H-matrix is divided by its corresponding element in the gains-matrix to cancel out unpredictable gain variations. The measurement procedure for the daily calibration is discussed in further detail in the Chapter 5.

The calculations described up to this point have constructed a single H-matrix, containing the complex gains for each of the 256 propagation channels. This process is repeated for each Fourier Transform block in the data stream, producing over one hundred H-matrices for each ten-second measurement. At least thirty-six measurements are recorded in a single local area and several local area points are measured in each environment, as described in Chapter 3. The correlation coefficient and theoretical MEA capacity parameters can be calculated from this body of data to produce a statistical representation of the channel.

Equation (4-9) is a reiteration of the MEA capacity calculation described in Chapter 3. It should be noted that this equation requires only one H-matrix, and does not relate elements from different H-matrices. Because a single H-matrix provides only one observation of the channel, and not a complete statistic representation, a large number of capacity calculations must be performed to find the minimum, maximum and mean capacity values. These stochastic parameters may then be used to compare the potential system capacity of different locations and predict system performance in similar environments. This expression was introduced in Chapter 3 and denotes the number of transmitter antennas as "n_T" and the system's signal-to-noise ratio as "ρ_{SYS}":

$$C = \log_2\left[\det\left(I + \frac{\rho_{SYS}}{n_T} HH^t\right)\right] \quad \textbf{(4-9)}$$

The correlation coefficient describes the similarity of two fading channels, as defined by two pairs of transmitter and receiver antenna elements and represented as two elements of an H-matrix. As discussed in Chapter 3, a pair of sequences is constructed from the two elements in each H-matrix from a local area measurement, and a single correlation coefficient is calculated for the two channels. Unlike the system capacity expression, the correlation coefficient function uses elements from many independent H-matrices. Equation (4-10) is used to calculate the correlation coefficient from two vectors of H-matrix elements.

$$\rho = \frac{R_{XY}(0) - \mu_X \mu_Y}{\sigma_X \sigma_Y} \quad \textbf{(4-10)}$$

Calculations have been discussed which transform sampled data from sixteen receiver antennas into values of correlation and system capacity. The data sampled from each receiver signal chain is multiplexed and stored to disk using LabView software. The data is then reorganized into matrices in which each column represents the waveform from a receiver antenna over a short period of time. Using the Discrete Fourier Transform, the complex spectrum is calculated from each received data stream. The amplitude values of the narrowband transmitted signals are picked from the spectrum and then normalized to remove non-ideal gain and phase distortion of the measurement system. The resulting amplitude values are combined into an H-matrix. Parameters are calculated with these H-matrices which describe the gain of multiple-antenna communication systems over a single-antenna system in the measured environment.

4.6 Summary

The measurement system described in this chapter is able to detect the fading coefficients between sixteen transmitter and sixteen receiver antenna elements. The transmitter consists of sixteen independent signal chains, and each chain produces a signal at one element on a transmitter antenna array. Each signal is a narrowband tone, and each

transmitter antenna element is distinguished at the receiver by a specific carrier frequency. The receiver also contains a sixteen-element array, and together the two arrays produce 256 propagation channels. The signal from each receiver element is downconverted, filtered and sampled with independent signal chains. The ray data from each element is stored to disk and later processed to produce a number of H-matrices, representing the gains of the propagation channels. The H-matrices are then input into correlation and capacity calculations to produce statistical parameters of the propagation environment.

As a note, the system uses a transmitter frequency of 2.111GHz because Lucent Technologies currently owns a national experimental license at this frequency, and because no commercial systems transmit within this band. Measurements were conducted prior to system construction to verify that no significant interfering signals were in this 32kHz bandwidth in Blacksburg, Virginia. In addition, the proximity of this transmit frequency to the 2.4GHz industrial, scientific and medical (ISM) band suggest that measurements with this system may be applicable to commercial wireless communication systems. The ISM frequency band is currently used for IEEE 802.11 wireless LAN and Bluetooth applications.

Significant aspects of the design and implementation of the measurement system were discussed. A narrow transmit bandwidth simplified the design process by easing gain flatness requirements of the individual components. GPS receivers were chosen in favor of more complicated phase-lock mechanisms to ensure frequency stability in the data, and a direct-downconversion receiver architecture was implemented to minimize component count and oscillator phase-noise. These design characteristics were implemented to ensure isolation between signal chains and a high signal-to-noise ratio in the processed data. Figures (4-15) and (4-16) depict the completed transmitter and receiver subsystems. The antenna arrays, backup battery supplies and the portable computer are indicated.

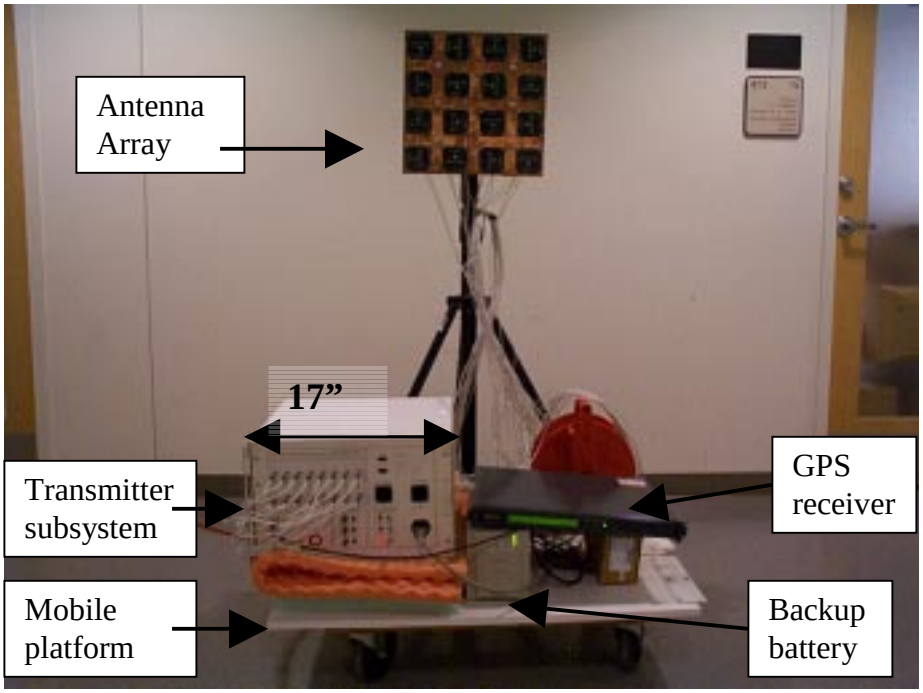

Figure 4-15: Photograph of the transmitter unit on the mobile platform. Significant components are labeled.

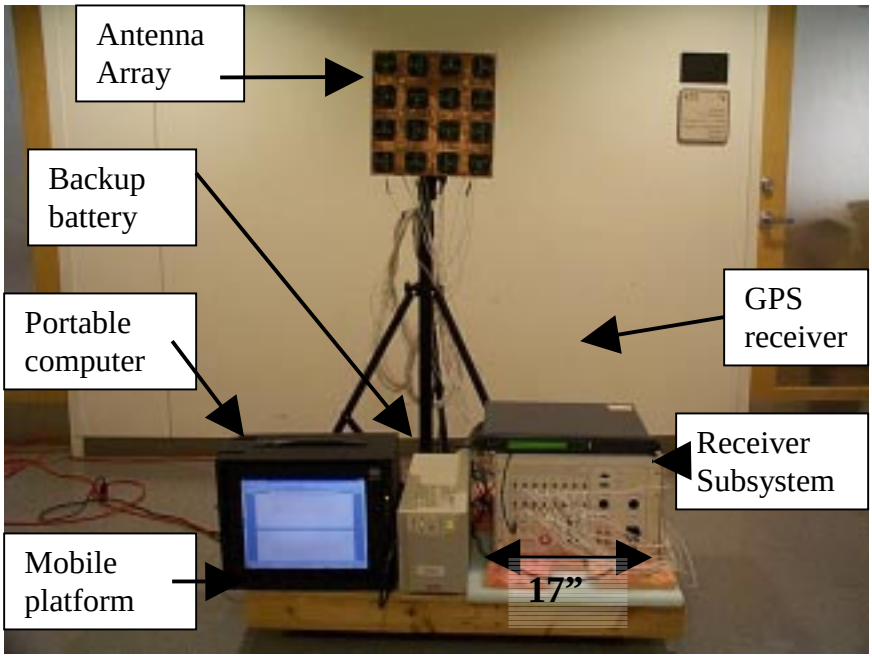

Figure 4-16: Photograph of the receiver unit on the mobile platform. Significant components are labeled.